Organellar Glue: A Molecular Tool to Artificially Control Chloroplast–Chloroplast Interactions

Ichikawa, Shintaro; Kato, Shota; Fujii, Yuta; Ishikawa, Kazuya; Numata, Keiji; Kodama, Yutaka

ACS SyntheticBiology

pubs.acs.org/synthbio Letter

Organellar Glue: A Molecular Tool to Artificially Control Chloroplast−Chloroplast Interactions

Shintaro Ichikawa,[⊥] Shota Kato,[⊥] Yuta Fujii, Kazuya Ishikawa, Keiji Numata, and Yutaka Kodama*

Cite This: *ACS Synth. Biol.* 2022, 11, 3190−3197 Read Online

ACCESS | Metrics & More | Article Recommendations | Supporting Information

ABSTRACT: Organelles can physically interact to facilitate various cellular processes such as metabolite exchange. Artificially regulating these interactions represents a promising approach for synthetic biology. Here, we artificially controlled chloroplast−chloroplast interactions in living plant cells with our organelle glue (ORGL) technique, which is based on reconstitution of a split fluorescent protein. We simultaneously targeted N-terminal and C-terminal fragments of a fluorescent protein to the chloroplast outer envelope membrane or cytosol, respectively, which induced chloroplast−chloroplast interactions. The cytosolic C-terminal fragment likely functions as a bridge between two N-terminal fragments, thereby bringing the chloroplasts in close proximity to interact. We modulated the frequency of chloroplast−chloroplast interactions by altering the ratio of N- and C-terminal fragments. We conclude that the ORGL technique can successfully control chloroplast−chloroplast interactions in plants, providing a proof of concept for the artificial regulation of organelle interactions in living cells.

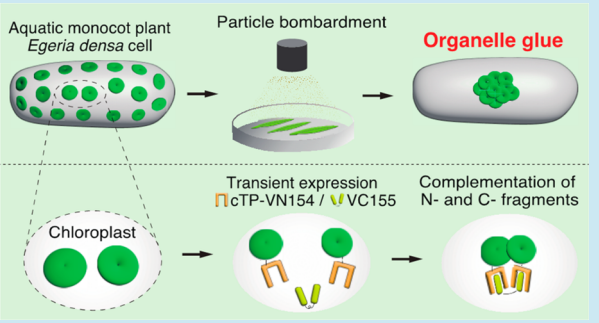

KEYWORDS: *bimolecular fluorescence complementation (BiFC), chloroplasts, Egeria densa, mitochondria, organelle interaction, peroxisome*

INTRODUCTION

Plant organelles physically interact to facilitate many cellular processes in response to changes in environmental conditions. Chloroplast−chloroplast interactions, also known as chloroplast aggregation, are induced in response to cold temperatures in diverse plant species such as the liverworts *Marchantia polymorpha* and *Apopellia endiviifolia*, the Southern maidenhair fern (*Adiantum capillus-veneris*), and the gymnosperm Japanese yew (*Taxus cuspidata*).[1−4] In the light, chloroplasts physically interact with peroxisomes and mitochondria.[5,6] Various organelles, such as chloroplasts, mitochondria, and peroxisomes, share metabolic pathways and appear to exchange metabolites via direct physical contact.[7] The artificial control of these organellar interactions would offer means to manipulate metabolic pathways such as photorespiration for basic research or engineering purposes. Although the artificial regulation of organellar interactions represents a promising approach for synthetic biology, techniques to modulate these key interactions remain to be developed.

Bimolecular fluorescence complementation (BiFC) assays allow the visualization of protein−protein interactions in a variety of living cells.[8,9] BiFC is based on the structural reconstitution of a functional fluorescent protein between two nonfluorescent N- and C-terminal fragments of a fluorescent protein (e.g., green fluorescent protein [GFP], red fluorescent protein [RFP], and other variants). To detect such protein−protein interactions, the nonfluorescent N- and C-terminal fragments are individually fused to the proteins of interest; the encoding constructs are then coexpressed in living cells. If the two proteins fused to each fragment of the fluorescent protein interact, they will bring the N-terminal and C-terminal fragments in proximity, allowing the reconstitution of the full-length functional protein, resulting in fluorescence.[8,9] During this structural reconstitution, the N-terminal fragment is integrated within the C-terminal fragment via the formation of hydrophobic interactions and a hydrogen bond network. For example, GFP and its variants, such as the monomeric yellow fluorescent protein mVenus, are composed of 11 β-strands and can be split into two fragments: VN154 (β-strands 1 to 7, amino acids 1−154) and VC155 (β-strands 8 to 11, amino acids 155−239). The inner face of each mVenus fragment is hydrophobic; when present in the same cell, the hydrophobic faces of VN154 and VC155 are thus attracted to and interact with each other, and a hydrogen bond network forms between VN154 and VC155. During this interaction, β-strand 7 of

Received: July 11, 2022
Published: September 30, 2022

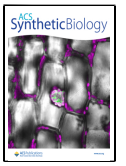

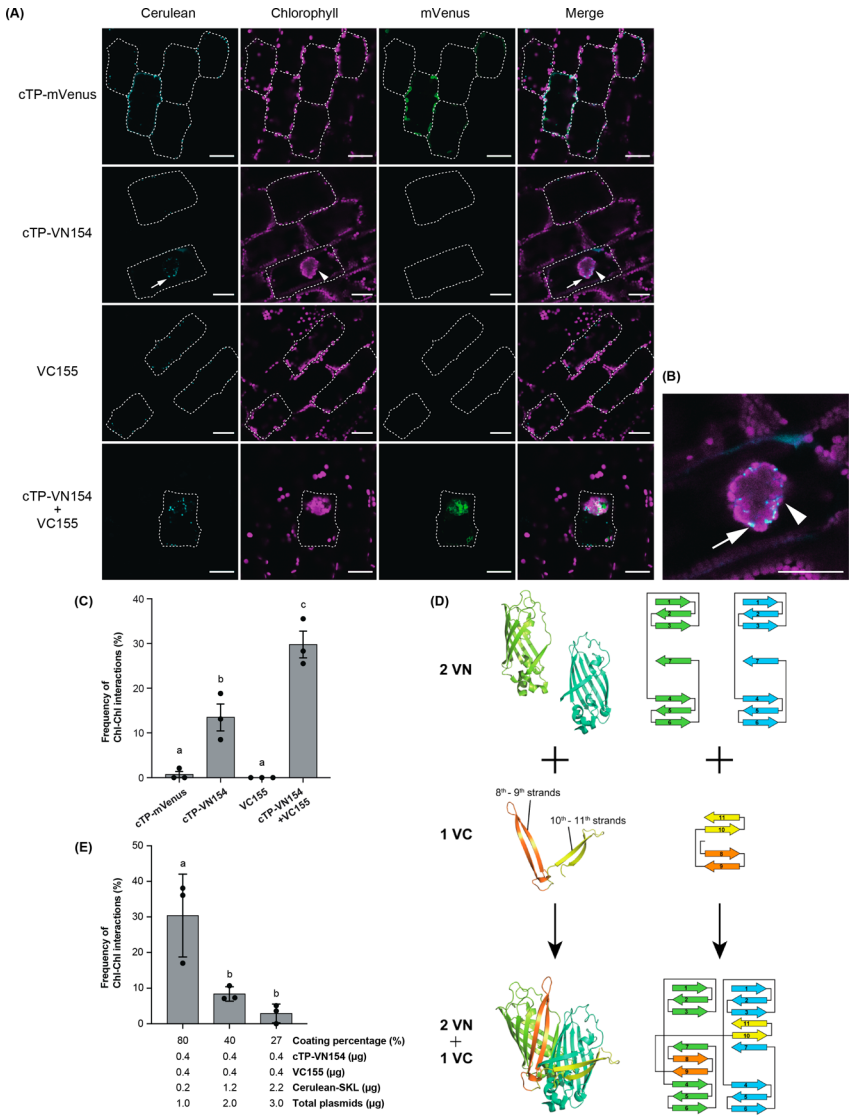

Figure 1. Chloroplast−chloroplast interactions via BiFC-based organelle glue (ORGL). (A) Chloroplast−chloroplast interactions in *Egeria densa* cells expressing *cTP-VN154* only or coexpressing *cTP-VN154* and *VC155*. *cTP-mVenus* and *VC155* were used as controls. White dashed lines show the outline of the bombarded cells, based on fluorescence of the Cerulean-SKL marker. White arrowheads indicate chloroplast−chloroplast interactions (aggregated chloroplasts). Arrow indicates peroxisomes. Scale bars, 30 μm. (B) Enlarged image of interacting chloroplasts in a cell expressing *cTP-VN154*. Magnified view of the cell shown in (A). The arrow and arrowhead indicate peroxisomes and chloroplast aggregates, respectively. Scale bar, 30 μm. (C) Frequency of chloroplast−chloroplast interactions in *E. densa* cells expressing the indicated constructs, *cTP-mVenus* (0.4 μg), *cTP-VN154* (0.4 μg), *VC155* (0.4 μg), or *cTP-VN154* (0.4 μg) + *VC155* (0.4 μg). The total plasmid amount in the coating was adjusted to 1.0 μg using pGWT35S-Cerulean-SKL plasmids (0.6 μg or 0.2 μg). The indicated constructs were mixed and coated onto 0.15 mg of gold particles. Data are means ± SD (n = 3). Chloroplast−chloroplast interactions were counted in cells expressing *cTP-mVenus*, *cTP-VN154*, *VC155*, or *cTP-VN154* + *VC155*. Different lowercase letters indicate significant differences (Tukey's multiple range test, $p < 0.05$). Chl−Chl, chloroplast−chloroplast. (D) Schematic illustration of the joining of the two different mVenus N-terminal fragments with the C-terminal fragment of mVenus. The protein structures (PDB: 1MYW) were visualized using PyMOL. (E) Frequency of chloroplast−chloroplast interactions in *E. densa* cells bombarded with gold particles coated with different amounts of the ORGL plasmids pGWT35S-cTP-VN154 and pGWT35S-VC155. pGWT35S-Cerulean-SKL competed with the ORGL plasmids, inhibiting the coating of the ORGL plasmids onto gold particles. The coating percentage (%) for the two ORGL plasmids was calculated by dividing the sum of the concentrations (0.8 μg [0.4 μg each]) of the ORGL plasmids by the total plasmid amount (1, 2, or 3 μg). The indicated plasmids were mixed and coated onto 0.15 mg of gold particles. Chloroplast−chloroplast interactions were scored in cells expressing the ORGL plasmids: the coating percentages were 80%, 40%, and 27%, respectively. Data are means ± SD (n = 3). Different lowercase letters indicate significant differences (Tukey's multiple range test, $p < 0.05$). Chl−Chl, chloroplast−chloroplast.

VN154 intercalates itself between the two β-sheets (consisting of β-strands 8−9 and 10−11) of VC155, akin to a key in a keyhole, which increases the frequency of structural reconstitution.[10] Because of the robustness of the hydrophobic interactions and hydrogen bond network, structural reconstitution during BiFC is irreversible.[8] Importantly, when only the free N- and C-terminal fragments of the fluorescent protein accumulate in the same cell, a BiFC reaction also occurs due to random oscillations and self-assembly.[9] This self-assembly is an undesired reaction during typical protein−protein interaction analyses, as it enhances background fluorescence and may result in false positives.[9]

In this study, we harnessed the irreversible self-assembly feature of BiFC to induce irreversible organelle interactions.

https://doi.org/10.1021/acssynbio.2c00367
ACS Synth. Biol. 2022, 11, 3190−3197

Using living plant cells, we induced irreversible BiFC reactions that brought different chloroplasts in close proximity and succeeded in artificially controlling the frequency and degree of these chloroplast−chloroplast interactions. This BiFC-based approach has great potential, not only for visualizing protein−protein interactions but also for regulating organellar interactions in living cells.

RESULTS AND DISCUSSION

To develop a technique to artificially induce chloroplast−chloroplast interactions, we took advantage of the hydrophobic feature of the VN154 fragment of mVenus, which consists of the first seven β-strands (β-strands 1−7) of the protein. We hypothesized that a VN154 molecule would stick to other VN154 molecules via hydrophobic interactions. As a negative control, we used full-length mVenus, comprising all 11 β-strands with a hydrophobic core protected from outside interactions. We added a transit peptide to target VN154 and mVenus to the chloroplast outer membrane (cTP: amino acids 1−50 from *Arabidopsis* [*Arabidopsis thaliana*] chloroplast OUTER ENVELOPE MEMBRANE PROTEIN7 [OEP7; encoded by At3g52420])[11] and transiently expressed the resulting *cTP-VN154* and *cTP-mVenus* constructs via particle bombardment in the aquatic monocot plant Brazilian waterweed (*Egeria densa*), whose chloroplasts are easily observed by microscopy.[12] To identify the transformed cells, we cobombarded plants with the pGWT35S-Cerulean-SKL plasmid, encoding a peroxisome-localized Cerulean fluorescent protein (Cerulean-SKL) as a marker. In cells expressing *cTP-VN154* alone, we observed that different chloroplasts interact and form aggregates resembling spheres (Figure 1A). Note that the chloroplast aggregate contained peroxisomes (Figure 1B). Of the cells expressing the *cTP-VN154* construct, 13.6% showed chloroplast−chloroplast aggregation (Figure 1C and Table 1).

Table 1. Frequency of Chloroplast−Chloroplast (Chl−Chl) Interactions in *E. densa* Cells Accumulating the Indicated Proteins

expressed proteins	trial	number of observed cells	number of cells with Chl−Chl interactions	frequency (%)
cTP-mVenus	#1	48	1	0.7 ± 1.2
	#2	78	0	
	#3	55	0	
cTP-VN154	#1	69	13	13.6 ± 5.2
	#2	60	8	
	#3	47	4	
VC155	#1	59	0	0
	#2	64	0	
	#3	64	0	
cTP-VN154 VC155	#1	55	14	30.3 ± 6.1
	#2	62	23	
	#3	53	15	

By contrast, we detected almost no chloroplast−chloroplast aggregation in cells expressing *cTP-mVenus* alone (Figure 1A,C, and Table 1). We reasoned that the chloroplast−chloroplast aggregative interactions might have formed via interactions between the hydrophobic region of distinct VN154 molecules.

We also determined that the frequency of chloroplast−chloroplast aggregation can be raised when cells coexpress constructs encoding cytosolic VC155 and chloroplast-localized cTP-VN154. We found not only the complemented fluorescence at the chloroplast periphery, but also the increased frequency of chloroplast−chloroplast aggregation to 30.3% over that seen with the expression of *cTP-VN154* alone under these conditions (Figure 1A,C, and Table 1). Because cytosolic VC155 alone did not induce chloroplast−chloroplast aggregation (Figure 1C and Table 1), we considered that cytosolic VC155 might function as a bridge between two VN154 molecules located at the outer membranes of different chloroplasts. VC155 (β-strands 8−11) is structurally split into two β-sheets (β-strands 8−9 and 10−11) (Figure 1D), while β-strands 7−10 of mVenus are flexible, based on molecular simulations of the folding of GFP.[13] Each β-sheet of VC155 might therefore become intercalated with different VN154 molecules at the chloroplast outer membrane (Figure 1D), raising the frequency of chloroplast−chloroplast aggregative interactions. Although Figure 1D shows the conceptual and simplified illustration of two VN154 fragments and one VC155 fragment as a bridge, each VN154 molecule may also function as a bridge between two different VC155 molecules, resulting in the formation of oligomers (Figure S1). Indeed, Venus reassembled by BiFC was shown to form oligomers in *Escherichia coli*.[14] Taken together with our data, cTP-VN154 and VC155 appeared to not only reconstitute mVenus monomers, but also form oligomers at the chloroplast periphery. Regardless of the exact mechanism, we succeeded in artificially inducing chloroplast−chloroplast interactions via BiFC between cTP-VN154 and VC155. We named this BiFC-based system for inducible organelle interaction the "organelle glue" (ORGL) technique.

To attempt to control the frequency of chloroplast−chloroplast aggregative interactions using the ORGL technique, we changed the relative amounts of ORGL plasmids (pGWT35S-cTP-VN154 and pGWT35S-VC155) introduced into each cell. Considering the sizes of gold particles used for bombardment (1 μm in diameter) and plasmid DNA (hundreds of nanometers),[15] a single gold particle should be coated with many copies of the plasmids prior to bombardment. We tested different amounts of VN154- and VC155-encoding plasmids by altering the amount of pGWT35S-Cerulean-SKL added to the plasmid mixture, as it will compete with the ORGL plasmids during the coating of gold particles, whose numbers remained constant. The frequency of chloroplast−chloroplast aggregation increased when more ORGL plasmids (resulting from lower pGWT35S-Cerulean-SKL amounts) were used to coat the gold particles (Figure 1E and Table 2), confirming the prediction that the chloroplast−chloroplast aggregative interaction is caused by the introduction of ORGL plasmids.

As mentioned above, VC155 appeared to act as a bridge between two VN154 fragments (Figure 1D). If true, a higher ratio of VC155 plasmid relative to cTP-VN154 plasmid DNA should increase the frequency of chloroplast−chloroplast aggregative interactions, while more cTP-VN154 plasmid DNA relative to that of VC155 would result in the opposite effect. To test this hypothesis, we maintained the amount of cTP-VN154 (0.4 μg each) while changing the amount of VC155 (0.13, 0.4, or 1.2 μg), yielding three different cTP-VN154:VC155 ratios (1:0.3, 1:1, and 1:3, respectively) (Figure 2A and Table 3). The 1:0.3 and 1:1 ratios between the two plasmid DNA amounts induced similar frequencies of chloroplast−chloroplast aggregation, and a 1:3 ratio between cTP-VN154 and VC155 significantly increased this frequency

https://doi.org/10.1021/acssynbio.2c00367
ACS Synth. Biol. 2022, 11, 3190−3197

Table 2. Frequency of Chloroplast−Chloroplast (Chl−Chl) Interactions in *E. densa* Cells Bombarded with Gold Particles Coated with Different Amounts of ORGL Plasmids

coating percentage (%)	trial	number of observed cells	number of cells with Chl−Chl interactions	frequency (%)
80	#1	42	16	30.4 ± 11.6
	#2	36	13	
	#3	53	9	
40	#1	56	6	8.4 ± 2.0
	#2	42	3	
	#3	55	4	
27	#1	28	1	2.9 ± 2.6
	#2	49	0	
	#3	59	3	

3.8- and 9.1-fold over that seen with the 1:0.3 and 1:1 ratios, respectively (Figure 2A and Table 3). These results suggest that VC155 acts as a bridge between two VN154 fragments and that the frequency of chloroplast−chloroplast aggregative interactions can be controlled by altering the ratio of VC155 to cTP-VN154 plasmid DNA used for bombardment.

To better quantify chloroplast−chloroplast aggregation induced by cTP-VN154 and VC155, we developed a sensitive metric, in contrast to the binary cell counting method used above. Accordingly, we assessed chloroplast distribution by measuring the angle (deg) formed between each chloroplast and the cell centroid as vertex to the polar axis of the cell Cartesian coordinates (Figure 2B). The angle value will depend on chloroplast distribution within the cell: In a cell without chloroplast−chloroplast aggregation, varied angles should be obtained (Figure 2B). By contrast, in a cell exhibiting chloroplast−chloroplast aggregation, chloroplasts should display similar angles to the cell centroid (Figure 2B). To estimate the extent of chloroplast aggregation, we turned to the standard deviation of angles for each cell, with a lower standard deviation being indicative of a higher degree of chloroplast−chloroplast aggregation. Using the same cells imaged above with three different ratios of cTP-VN154:VC155 plasmid DNA (1:0.3, 1:1, and 1:3), we measured the angles between individual chloroplasts and the cell centroid, followed by the calculation of the corresponding standard deviations. The median standard deviation decreased as the ratio increased (Figure 2C). This method can therefore be used to quantify the degree of chloroplast−chloroplast aggregation.

We also tested whether the chloroplast−chloroplast aggregates formed by cTP-VN154 and VC155 might contain other organelles (peroxisomes, mitochondria, and nuclei), based on the observation that cTP-VN154-mediated chloroplast−chloroplast aggregation traps peroxisomes (Figure 1B). As with cTP-VN154 alone, the chloroplast−chloroplast aggregates formed by the coexpression of *cTP-VN154* and *VC155* contained peroxisomes, which we labeled with Cerulean-SKL (Figure 3). We also observed mitochondria within the chloroplast−chloroplast aggregates, when mitochondria were labeled with mCherry harboring a mitochondrial targeting peptide (mTP-mCherry) (Figure 3). By contrast, the chloroplast−chloroplast aggregates did not contain the nucleus, which we labeled with mCherry fused to a nuclear localization signal (mCherry-NLS) (Figure 3). In sum, the chloroplast−chloroplast aggregates formed by cTP-VN154 and VC155 contained peroxisomes and mitochondria, but not the nucleus. Because these three organelles

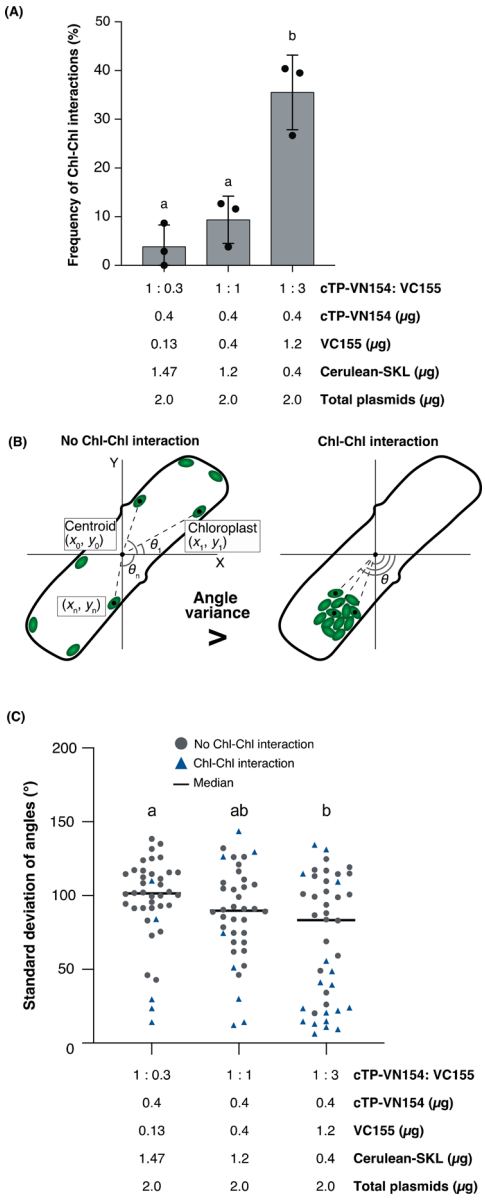

Figure 2. The frequency of chloroplast−chloroplast interactions can be controlled. (A) Frequency of chloroplast−chloroplast interactions in *E. densa* cells bombarded with particles coated with the ORGL plasmids (pGWT35S-cTP-VN154 and pGWT35S-VC155) in different ratios (1:0.3, 1:1, and 1:3). The amount of pGWT35S-cTP-VN154 was constant, while that of pGWT35S-VC155 changed. The indicated plasmids were mixed and coated onto 0.15 mg of gold particles. Cells showing chloroplast−chloroplast interactions were counted when expressing the ORGL plasmids for *cTP-VN154* and *VC155* at 1:0.3, 1:1, and 1:3 ratios. Data are means ± SD (n = 3). Different lowercase letters indicate significant differences (Tukey's multiple range test, $p < 0.05$). Chl−Chl, chloroplast−chloroplast. (B) Schematic illustration of the quantification of degree (θ) relative to the cell centroid for chloroplast−chloroplast aggregation in *E. densa* cells. Chl−Chl, chloroplast−chloroplast. (C) Quantification of degree for chloroplast−chloroplast aggregation. Different lowercase letters show significant differences (Kruskal−Wallis test, $p < 0.05$). Chl−Chl, chloroplast−chloroplast.

(chloroplasts, peroxisomes, and mitochondria) participate in photorespiration and exchange metabolites,[16,17] the ORGL technique may allow the modulation of metabolic flow when using cTP-VN154 and VC155. Thus, the ORGL technology

https://doi.org/10.1021/acssynbio.2c00367
ACS Synth. Biol. 2022, 11, 3190−3197

Table 3. Frequency of Chloroplast−Chloroplast (Chl−Chl) Interactions in *E. densa* Cells Bombarded with Particles Coated with ORGL Plasmids at Different Ratios

ratio (cTP-VN154:VC155)	trial	number of observed cells	number of cells with Chl−Chl interactions	frequency (%)
1:0.3	#1	41	0	3.9 ± 4.4
	#2	46	4	
	#3	34	1	
1:1	#1	43	5	9.4 ± 4.9
	#2	53	2	
	#3	55	7	
1:3	#1	45	12	35.5 ± 7.7
	#2	38	15	
	#3	47	19	

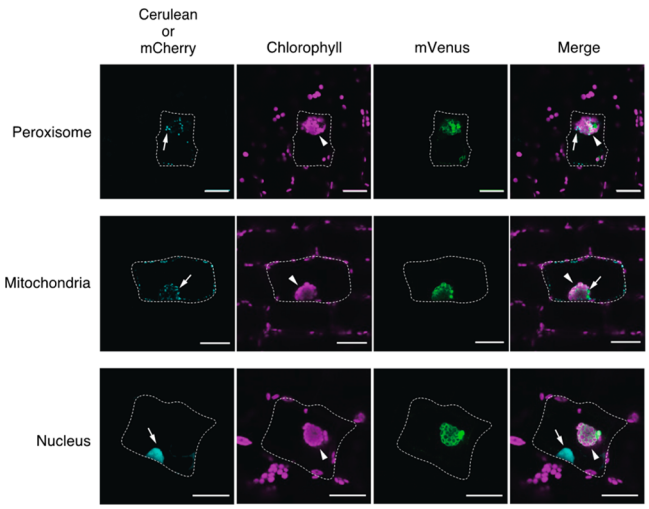

Figure 3. Incorporation of organelles into aggregated chloroplasts. Representative examples of the localization of peroxisomes, mitochondria, and nuclei in bombarded *E. densa* cells showing chloroplast−chloroplast interactions. Peroxisomes were visualized by Cerulean (pGWT35S-Cerulean-SKL [0.2 μg]), and mitochondria and nucleus were visualized by mCherry (pGWT35S-mTP-mCherry [0.2 μg] and pGWT35S-mCherry-NLS [0.2 μg], respectively). To induce chloroplast−chloroplast interactions, the ORGL plasmids (pGWT35S-cTP-VN154 [0.4 μg] and pGWT35S-VC155 [0.4 μg]) were used. The plasmid mix (total 1.0 μg) was coated onto 0.15 mg of gold particles. Chloroplasts were detected by chlorophyll autofluorescence. Arrows indicate peroxisomes, mitochondria, and nucleus, and arrowheads indicate chloroplast aggregates. Scale bars, 30 μm.

has the potential to contribute to the study of interactions consisting not only of one organelle type (e.g., the interaction between chloroplasts), but also of multiple organelle types (e.g., the interaction between chloroplasts, peroxisomes, and mitochondria).

The expression of *cTP-VN154* alone and the coexpression of *cTP-VN154* and *VC155* induced chloroplast−chloroplast aggregative interactions (Figure 1A,C). To further explore the potential of the ORGL technique, we tested several VN154 and VC155 fragments (Table S1). We observed no chloroplast−chloroplast aggregation when a construct encoding cytosolic VN154 was expressed alone or together with a construct encoding cytosolic VC155 (Table S1). We also coexpressed *cTP-VN154* and *cTP-VC155* constructs to localize both VN154 and VC155 fragments to the chloroplast outer membrane, which induced chloroplast−chloroplast aggregation (10.7%) (Table S1). The aggregation efficiency obtained from the coexpression of *cTP-VN154* and *cTP-VC155* was similar to that seen with *cTP-VN154* alone (13.6%) (Figure 1C and Table 1). Because the VC155 fragment also has a hydrophobic region, we tested whether cTP-VC155 alone might induce chloroplast aggregation. Indeed, cTP-VC155 alone also induced chloroplast−chloroplast aggregative interactions (15.7%) (Table S1). The efficiency of cTP-VC155 alone was similar to that measured for cTP-VN154 alone (13.6%) (Figure 1C and Table 1). However, the coexpression of *cTP-VC155* with *VN154* encoding the cytosolic form of VN154 caused a sharp decrease in the frequency of the chloroplast−chloroplast aggregation (0.7%) (Table S1). We anticipate that the *cTP-VC155* and *VN154* constructs could potentially function as an ORGL variant to prevent organellar interactions.

To conclude, we developed the BiFC-based ORGL technique to artificially control chloroplast−chloroplast interactions in plant cells and provided a proof of concept in this study for the artificial regulation of organellar interactions in living organisms. We envisage that interactions between other organelles could also be controlled using the ORGL technique by modifying the signal peptides fused to the VN154 and VC155 fragments. Hence, BiFC technology can not only visualize protein−protein interactions but also regulate organellar interactions.

The ORGL technique is based on the irreversible reconstitution of a fluorescent protein structure. The underlying BiFC reaction between the two fragments of a fluorescent protein occurs via hydrophobic interactions and a network of hydrogen bonds. We hypothesize that the molecule-based glue reactions described here occur via other chemical interactions, such as electrostatic and covalent interactions. By taking advantage of various chemical interactions, the ORGL technology may be expanded in the future.

In plant cells, organellar interactions have been observed in response to changes in ambient environmental conditions such as light and temperature.[1−6] These organellar interactions, driven by changes in the surrounding environment, are involved in various cellular processes, such as metabolite exchange, but their exact roles were unknown due to the lack of a means of artificially manipulating interactions between organelles. The ORGL technology will pave the way to studying metabolite exchange mediated by organellar interactions.

METHODS

Plant Materials. Plants of the aquatic monocot *Egeria densa* were purchased from the aquarium store Kanseki Co., Ltd. (Utsunomiya, Japan) and cultured in fresh water under natural sunlight (approximately 25 μmol photons m^{-2} s^{-1}) at room temperature (22−25 °C) in the laboratory for use in particle bombardment.

Plasmid Construction. To construct pGWT35S-AtOEP7$^{1-50}$-mVenus, the sequence encoding amino acids 1−50 of *Arabidopsis* OEP7 (OEP7$^{1-50}$) was amplified by PCR, using pGWT35S-OEP7-mCherry[12] as template and the primers 5′-AACCAATTCAGTCGACATGGGAAAAACTTC-GGGA-3′ and 5′-ACCGCCGCTACCGCCGTCATCGGGG-TCTTTGGT-3′. The sequence encoding mVenus (Venus-A206K variant) was amplified by PCR using a synthetic *mVenus* gene (obtained from Eurofins Genomics) as template and the primers 5′-GGCGGTAGCGGCGGTATGGT-

https://doi.org/10.1021/acssynbio.2c00367
ACS Synth. Biol. 2022, 11, 3190−3197

GAGCAAGGGCGAG-3′ and 5′-AAGCTGGGTCTAGAT-ATCTTACTTGTACAGCTCGTC-3′. The two PCR products were fused by overlapping PCR with the primers 5′-AACCAATTCAGTCGACATGGGAAAAACTTCGGGA-3′ and 5′-AAGCTGGGTCTAGATATCTTACTTGTACAG-CTCGTC-3′, producing the DNA fragment encoding AtOEP7$^{1-50}$-mVenus. The amplicon was cloned into pEN-TR1A by In-Fusion Cloning (Clontech) after *Sal*I and *Eco*RV digestion, generating pENTR1A-AtOEP7$^{1-50}$-mVenus.

To construct pGWT35S-AtOEP7$^{1-50}$-VN154, the *AtOEP7*$^{1-50}$ sequence was amplified by PCR using pMpGWB106-OEP7(1−50)[3,11] as template and the primers 5′-GGGGACAAGTTTGTACAAAAAAGCAGGCTC-CATGGGAAAAACTTCGGG-3′ and 5′-ACCTCCAGAG-CCACCGTCATCGGGGTCTTTGGTTG-3′. The DNA fragment encoding the N-terminal region of mVenus (amino acids 1−154, VN154)[18,10] was amplified by PCR with the primers 5′-GGTGGCTCTGGAGGTATGGTGAGCAAGGGC-3′ and 5′-GGGGACCACTTTGTACAAGAAAGCTGGGTC-TCAGGCGGTGATATAGACG-3′. The two PCR products were fused by overlapping PCR with the primers 5′-GGGGACAAGTTTGTACAAAAAAGCAGGCTCCATGG-GAAAAACTTCGGG-3′ and 5′-GGGGACCACTTTGTA-CAAGAAAGCTGGGTCTCAGGCGGTGATATAGACG-3′, producing the DNA fragment *AtOEP7*$^{1-50}$*-VN154*. The amplicon was cloned into pDONR207 by Gateway BP reaction (Invitrogen), generating pDONR207-AtOEP7$^{1-50}$-VN154.

To construct pGWT35S-AtOEP7$^{1-50}$-VC155, the sequence of *AtOEP7*$^{1-50}$ was amplified by PCR with pGWT35S-OEP7-mCherry[12] as template and the primers 5′-GGGGACAAGTT-TGTACAAAAAAGCAGGCTCCATGGGAAAAACTTC-GGG-3′ and 5′-ACCGCCGCTACCGCCGTCATCGGGG-TCTTTGGT-3′. The DNA fragment encoding the C-terminal region of mVenus (amino acids 155−238 including A206 K, VC155) was amplified by PCR with using a synthetic *mVenus* gene as template and the primers 5′-GGCGGTAGCG-GCGGTGTGGACAAGCAGAAGAAC-3′ and 5′-GGGGA-CCACTTTGTACAAGAAAGCTGGGTCTCACTTGTAC-AGCTCGTCC-3′. The two PCR products were fused by overlapping PCR with the primers 5′-GGGGACAAGT-TTGTACAAAAAAGCAGGCTCCATGGGAAAAACTT-CGGG-3′ and 5′-GGGGACCACTTTGTACAAGAAAGCT-GGGTCTCACTTGTACAGCTCGTCC-3′, producing the DNA fragment *AtOEP7*$^{1-50}$*-VC155*. The amplicon was cloned into pDONR207 by Gateway BP reaction (Invitrogen), generating pDONR207-AtOEP7$^{1-50}$-VC155.

To construct pGWT35S-VN154, the sequence of *VN154* was amplified by PCR using the synthetic *mVenus* gene as template and the primers 5′-GGGGACAAGTTTGTA-CAAAAAAGCAGGCTCCATGGTGAGCAAGGGCGAG-3′ and 5′-GGGGACCACTTTGTACAAGAAAGCTGGGTC-TCAGGCGGTGATATAGACG-3′. The resulting amplicon was cloned into pDONR207 by Gateway BP reaction (Invitrogen), generating pDONR207-VN154.

To construct pGWT35S-VC155, the sequence of *VC155* was amplified by PCR with the synthetic *mVenus* gene as template and the primers 5′-AACCAATTCAGTCGA-CATGGTGGACAAGCAGAAGAACGGC-3′ and 5′-AAGCTGGGTCTAGATATCTTACTTGTACAGCTCGT-CCATGCCGAGAGT-3′. The amplicon was cloned into pENTR1A by In-Fusion Cloning (Clontech) after *Sal*I and *Eco*RV digestion, generating pENTR1A-VC155.

To construct pGWT35S-Cerulean-SKL, the DNA fragment encoding Cerulean-SKL was amplified by PCR using a plasmid encoding Cerulean[10] as template and the primers 5′-GGGGA-CAAGTTTGTACAAAAAAGCAGGCTCCATGGTGAGC-AAGGGCGAG-3′ and 5′-GGGGACCACTTTGTACAAGA-AAGCTGGGTCTCACAACTTGGACTTGTACAGCTC-GTCC-3′ and cloned into pDONR207 by Gateway BP reaction, generating pDONR207-Cerulean-SKL.

To construct pGWT35S-AtTIM21$^{1-50}$-mCherry, the DNA fragment encoding amino acids 1−50 of the *Arabidopsis* TRANSLOCASE OF INNER MITOCHONDRIAL MEM-BRANE 21 (AtTIM21$^{1-50}$) homologue At4g00026[12,19] was amplified by PCR using pGWT35S-TIM21$^{1-50}$-Citrine[12] as template and the primers 5′-GGGGACAAGTTTGTA-CAAAAAAGCAGGCTCCATGATGATGATGAATCT-3′ and 5′-CGCCCTTGCTCACCATCTTTGAAAGAAATGA-3′. The *mCherry* sequence was amplified by PCR using pGWT35S-mCherry[12] as template and the primers 5′-TTTTAGCAACTCATTTCTTTCAAAGATGGTGAGCA-3′ and 5′-GGGGACCACTTTGTACAAGAAAGCTGGGTC-TCACTACTTGTACAGCTCG-3′. The two PCR products were fused by overlapping PCR with the primers 5′-GGGGACAAGTTTGTACAAAAAAGCAGGCTCCATGA-TGATGATGAATCT-3′ and 5′-GGGGACCACTTTGTA-CAAGAAAGCTGGGTCTCACTACTTGTACAGCTCG-3′, producing the DNA fragment *AtTIM21*$^{1-50}$*-mCherry*. This DNA fragment was cloned into pDONR207 by Gateway BP reaction (Invitrogen), generating pDONR207-AtTIM21$^{1-50}$-mCherry.

To construct pGWT35S-mCherry-NLS (nuclear localization signal[12,20]), the *mCherry-NLS* sequence was amplified by PCR using pGWT35S-mCherry[12] as template and the primers 5′-GGGGACAAGTTTGTACAAAAAAGCAGGCTTCATGG-TGAGCAAGGGCGAGGAGGA-3′ and 5′-GGGGACCACT-TTGTACAAGAAAGCTGGGTCTCACACCTTGCGCTT-CTTCTTAGGTCCCGACTTGTACAGCTCGTC-3′ and cloned into pDONR207 by Gateway BP reaction, generating pDONR207-mCherry-NLS.

The pENTR1A-AtOEP7$^{1-50}$-mVenus, pDONR207-AtOEP7$^{1-50}$-VN154, pDONR207-AtOEP7$^{1-50}$-VC155, pDONR207-VN154, pENTR1A-VC155, pDONR207-Cerulean-SKL, pDONR207-AtTIM21$^{1-50}$-mCherry, and pDONR207-mCherry-NLS plasmids were recombined with the pGWT35S vector[21] by Gateway LR reaction (Invitrogen), generating pGWT35S-AtOEP7$^{1-50}$-mVenus (pGWT35S-cTP-mVenus), pGWT35S-AtOEP7$^{1-50}$-VN154 (pGWT35S-cTP-VN154), pGWT35S-AtOEP7$^{1-50}$-VC155 (pGWT35S-cTP-VC155), pGWT35S-VN154, pGWT35S-VC155, pGWT35S-Cerulean-SKL, pGWT35S-AtTIM21$^{1-50}$-mCherry (pGWT35S-mTP-mCherry), and pGWT35S-mCherry-NLS, respectively.

Particle Bombardment. Particle bombardment of *E. densa* cells was performed as previously described.[12] Briefly, the BiFC plasmids and the control plasmid (pGWT35S-Cerulean-SKL for peroxisome visualization, pGWT35S-mTP-mCherry for mitochondria visualization, and pGWT35S-mCherry-NLS for nucleus visualization) were mixed in 11 μL of sterile water and coated onto 0.15 mg of gold particles (1 μm in diameter). Leaflets were detached from the plants and blotted dry with Kimwipes to remove excess water from their surfaces. The *E. densa* leaflets were then placed on a 1% (w/v) agar gel and subjected to particle bombardment using a biolistic PDS1000/He Particle Delivery System (Bio-Rad) with previously

https://doi.org/10.1021/acssynbio.2c00367
ACS Synth. Biol. 2022, 11, 3190−3197

reported conditions.[12] The bombarded leaves were incubated in the dark at 25 °C for 24 h.

Confocal Microscopy. The bombarded *E. densa* cells were examined under a confocal laser-scanning microscope (SP8X; Leica Microsystems) using the time-gating method.[22] mVenus fluorescence was observed with 510 nm excitation and 520−540 nm emission. mCherry fluorescence was observed with 585 nm excitation and 625−655 nm emission. The 510- and 585 nm lines of a white light laser were used (Leica Microsystems). When mVenus and mCherry fluorescence were detected, chlorophyll autofluorescence was rejected by time gating.[22] Cerulean fluorescence was observed with 458 nm excitation and 465−490 nm emission. Chlorophyll autofluorescence was observed with 458 nm excitation and 670−690 nm emission. The 458 nm laser line was from an argon laser.

Evaluation of Chloroplast−Chloroplast Interactions. To evaluate the frequency of chloroplast−chloroplast aggregation, the numbers of all bombarded cells (observed cells) and the cells exhibiting chloroplast−chloroplast aggregation were counted (Tables 1−3 and S1). The bombarded cells were identified based on fluorescence from the Cerulean-SKL marker. The frequency of chloroplast−chloroplast aggregation was calculated from the numbers obtained above. Experiments were repeated three times to obtain an average frequency and standard deviation.

To evaluate the degree of chloroplast−chloroplast aggregation, chloroplast distribution was quantified in each bombarded cell. The centroid of the transformed cell was determined by tracing the cell outline using the brightfield image (512 × 512 pixels) with Fiji image analysis software[23] and was used as the origin $[X_0, Y_0]$ in Cartesian coordinates. Next, the position of chloroplasts was marked using the brightfield and chlorophyll fluorescence images in Fiji. On the Cartesian coordinates (512 × 512 pixels), the coordinates of the chloroplast $[X_n, Y_n]$ were identified. The coordinates of two points, centroid $[X_0, Y_0]$ and chloroplast $[X_n, Y_n]$, were used to measure the angle (θ) of the chloroplast position, with the centroid as vertex to the polar axis. Chloroplast distribution was assessed by calculating the standard deviation of the angles.

■ ASSOCIATED CONTENT

Supporting Information

The Supporting Information is available free of charge at https://pubs.acs.org/doi/10.1021/acssynbio.2c00367.

> Frequency of chloroplast−chloroplast interactions in *Egeria densa* cells with several bombardment patterns (Table S1), and schematic illustration of the multimerization of multiple C-terminal mVenus fragments with multiple mVenus N-terminal fragments (Figure S1) (PDF)

■ AUTHOR INFORMATION

Corresponding Author

Yutaka Kodama − *Center for Bioscience Research and Education, Utsunomiya University, Tochigi 321-8505, Japan; Graduate School of Regional Development and Creativity, Utsunomiya University, Tochigi 321-8505, Japan; Biomacromolecules Research Team, Center for Sustainable Resource Science, RIKEN, Saitama 351-0198, Japan;* orcid.org/0000-0002-4720-7311; Email: kodama@cc.utsunomiya-u.ac.jp

Authors

Shintaro Ichikawa − *Center for Bioscience Research and Education, Utsunomiya University, Tochigi 321-8505, Japan; Graduate School of Regional Development and Creativity, Utsunomiya University, Tochigi 321-8505, Japan*

Shota Kato − *Center for Bioscience Research and Education, Utsunomiya University, Tochigi 321-8505, Japan*

Yuta Fujii − *Center for Bioscience Research and Education, Utsunomiya University, Tochigi 321-8505, Japan*

Kazuya Ishikawa − *Center for Bioscience Research and Education, Utsunomiya University, Tochigi 321-8505, Japan*

Keiji Numata − *Department of Material Chemistry, Graduate School of Engineering, Kyoto University, Kyoto 615-8510, Japan; Biomacromolecules Research Team, Center for Sustainable Resource Science, RIKEN, Saitama 351-0198, Japan;* orcid.org/0000-0003-2199-7420

Complete contact information is available at: https://pubs.acs.org/10.1021/acssynbio.2c00367

Author Contributions

K.N. and Y.K. conceptualized the study. S.K., Y.F., and Y.K. planned experiments. S.I., S.K., Y.F., and K.I. performed experiments. S.I., S.K., Y.F., and Y.K. performed data analysis. Y.K. wrote the first draft of the manuscript. S.I., S.K., and Y.K. prepared the figures and tables. All authors discussed the results and revised the manuscript.

Author Contributions

$^{\perp}$S.I. and S.K. contributed equally.

Notes

The authors declare no competing financial interest.

■ ACKNOWLEDGMENTS

The authors thank Ms. Rieko Saijo, Ms. Noriko Hamashima, Ms. Yuka Ogasawara, and Dr. Shoko Tsuboyama (Utsunomiya University) for technical assistance. This work was supported by the Japan Science and Technology Agency Exploratory Research for Advanced Technology (JST-ERATO; Grant Number JPMJER1602). Yutaka Kodama thanks the late Prof. Chang-Deng Hu (Purdue University), who passed away on September 1, 2022, for the initial development of BiFC technology (Hu et al. *Mol. Cell* **2002**, *9*, 789−798) and his guidance to date. May he rest in peace.

■ REFERENCES

(1) Tanaka, A. Photosynthetic Activity in Winter Needles of the Evergreen Tree *Taxus cuspidata* at Low Temperatures. *Tree Physiol.* **2007**, *27* (5), 641−648.

(2) Kodama, Y.; Tsuboi, H.; Kagawa, T.; Wada, M. Low Temperature-Induced Chloroplast Relocation Mediated by a Blue Light Receptor, Phototropin 2, in Fern Gametophytes. *J. Plant Res.* **2008**, *121* (4), 441−448.

(3) Tanaka, H.; Sato, M.; Ogasawara, Y.; Hamashima, N.; Buchner, O.; Holzinger, A.; Toyooka, K.; Kodama, Y. Chloroplast Aggregation during the Cold-Positioning Response in the Liverwort *Marchantia polymorpha*. *J. Plant Res.* **2017**, *130* (6), 1061−1070.

(4) Yong, L.; Tsuboyama, S.; Kitamura, R.; Kurokura, T.; Suzuki, T.; Kodama, Y. Chloroplast Relocation Movement in the Liverwort *Apopellia endiviifolia*. *Physiol. Plant.* **2021**, *173* (3), 775−787.

(5) Oikawa, K.; Matsunaga, S.; Mano, S.; Kondo, M.; Yamada, K.; Hayashi, M.; Kagawa, T.; Kadota, A.; Sakamoto, W.; Higashi, S.; Watanabe, M.; Mitsui, T.; Shigemasa, A.; Iino, T.; Hosokawa, Y.;

Nishimura, M. Physical Interaction between Peroxisomes and Chloroplasts Elucidated by in Situ Laser Analysis. *Nat. Plants* **2015**, *1* (4), 15035.
(6) Oikawa, K.; Imai, T.; Thagun, C.; Toyooka, K.; Ishikawa, K.; Kodama, Y.; Numata, K.; Yoshizumi, T. Mitochondrial Movement during Its Association with Chloroplasts in *Arabidopsis thaliana*. *Commun. Biol.* **2021**, *4*, 292.
(7) Bobik, K.; Burch-smith, T. M. Chloroplast Signaling within, between and beyond Cells. *Front. Plant Sci.* **2015**, *6*, 781.
(8) Hu, C. D.; Chinenov, Y.; Kerppola, T. K. Visualization of Interactions among BZIP and Rel Family Proteins in Living Cells Using Bimolecular Fluorescence Complementation. *Mol. Cell* **2002**, *9* (4), 789−798.
(9) Kodama, Y.; Hu, C. D. Bimolecular Fluorescence Complementation (BiFC): A 5-Year Update and Future Perspectives. *Biotechniques* **2012**, *53* (5), 285−298.
(10) Kodama, Y.; Hu, C. D. An Improved Bimolecular Fluorescence Complementation Assay with a High Signal-to-Noise Ratio. *Biotechniques* **2010**, *49* (5), 793−803.
(11) Lee, Y. J.; Kim, D. H.; Kim, Y.-W.; Hwang, I. Identification of a Signal That Distinguishes between the Chloroplast Outer Envelope Membrane and the Endomembrane System in Vivo. *Plant Cell* **2001**, *13* (10), 2175−2190.
(12) Osaki, Y.; Kodama, Y. Particle Bombardment and Subcellular Protein Localization Analysis in the Aquatic Plant *Egeria densa*. *PeerJ* **2017**, *5*, e3779.
(13) Reddy, G.; Liu, Z.; Thirumalai, D. Denaturant-Dependent Folding of GFP. *Proc. Natl. Acad. Sci. U. S. A.* **2012**, *109* (44), 17832−17838.
(14) Isogai, M.; Kawamoto, Y.; Inahata, K.; Fukada, H.; Sugimoto, K.; Tada, T. Structure and Characteristics of Reassembled Fluorescent Protein, a New Insight into the Reassembly Mechanisms. *Bioorg. Med. Chem. Lett.* **2011**, *21* (10), 3021−3024.
(15) Hansma, H. G.; Vesenka, J.; Siegerist, C.; Kelderman, G.; Morrett, H.; Sinsheimer, R. L.; Elings, V.; Bustamante, C.; Hansma, P. K. Reproducible Imaging and Dissection of Plasmid DNA under Liquid with the Atomic Force Microscope. *Science* **1992**, *256*, 1180−1184.
(16) Busch, F. A. Photorespiration in the Context of Rubisco Biochemistry, CO_2 Diffusion and Metabolism. *Plant J.* **2020**, *101*, 919−939.
(17) Oikawa, K.; Hayashi, M.; Hayashi, Y.; Nishimura, M. Re-Evaluation of Physical Interaction between Plant Peroxisomes and Other Organelles Using Live-Cell Imaging Techniques. *J. Integr. Plant Biol.* **2019**, *61* (7), 836−852.
(18) Shyu, Y. J.; Liu, H.; Deng, X.; Hu, C.-D. Identification of New Fluorescent Protein Fragments for Bimolecular Fluorescence Complementation Analysis under Physiological Conditions. *Biotechniques* **2006**, *40* (1), 61−66.
(19) Hamasaki, H.; Yoshizumi, T.; Takahashi, N.; Higuchi, M.; Kuromori, T.; Imura, Y.; Shimada, H.; Matsui, M. SD3, an *Arabidopsis thaliana* Homolog of TIM21, Affects Intracellular ATP Levels and Seedling Development. *Mol. Plant* **2012**, *5* (2), 461−471.
(20) Kalderon, D.; Roberts, B.; Richardson, W.; Smith, A. A Short Amino Acid Sequence Able to Specify Nuclear Location. *Cell* **1984**, *39*, 499−509.
(21) Fujii, Y.; Yoshimura, A.; Kodama, Y. A Novel Orange-Colored Bimolecular Fluorescence Complementation (BiFC) Assay Using Monomeric Kusabira-Orange Protein. *Biotechniques* **2018**, *64* (4), 153.
(22) Kodama, Y. Time Gating of Chloroplast Autofluorescence Allows Clearer Fluorescence Imaging in Planta. *PLoS One* **2016**, *11* (3), No. e0152484.
(23) Schindelin, J.; Arganda-Carreras, I.; Frise, E.; Kaynig, V.; Longair, M.; Pietzsch, T.; Preibisch, S.; Rueden, C.; Saalfeld, S.; Schmid, B.; Tinevez, J.-Y.; White, D. J.; Hartenstein, V.; Eliceiri, K.; Tomancak, P.; Cardona, A. Fiji - an Open Source Platform for Biological Image Analysis. *Nat. Methods* **2012**, *9*, 676−682.

https://doi.org/10.1021/acssynbio.2c00367
ACS Synth. Biol. 2022, 11, 3190−3197